Estimating Point of Contact, Force and Torque in a Biomimetic Tactile Sensor with Deformable Skin

Chia-Hsien Lin, *Student Member,* IEEE, Jeremy A. Fishel, *Member,* IEEE
and Gerald E. Loeb, *Senior Member, IEEE*

***Abstract*— The human fingertip is exquisitely sensitive to touch. Tactile information sensed by the mechanoreceptors of the fingertip make it possible to deduce information such as the location of contact and the normal forces, shear forces and torques being applied to the skin. Humans use this information to grasp and handle objects with great dexterity. Robotic systems seeking to obtain similar performance would benefit from these sensory capabilities. We have previously developed a multimodal tactile sensor – the BioTac®. Normal and shear forces are encoded by changes in the impedance of electrodes distributed over the core of the BioTac when the overlying elastomeric skin and conductive liquid deform. Previous studies have employed machine learning to quantify the relationship between sensory values and tri-axial force. In this study we present analytical methods that successfully estimate point of contact, tri-axial force and torque during contact with the BioTac. Estimating shear force and torque separately when they occur simultaneously remains challenging.**

I. Introduction

A. Human cutaneous touch capabilities

In human glabrous skin there are four types of mechanoreceptors each responding to different mechanical stimuli classified by their receptive field sizes and temporal responses [1-3]. Among them, two are classified as slowly adapting (Merkel disk receptors and Ruffini endings), providing sustained firing rates in response to continuous loads [4]. The Merkel disk receptors (type SA-I afferents) are located near the surface of the skin at the boundary of the dermal and epidermal tissues. They provide the largest responses to strains normal to the skin's surface [5] with a high spatial resolution [6] that would be useful for determining the point of contact. The Ruffini endings (type SA-II afferents) are located deeper in the subcutaneous tissue and provide the greatest response to skin stretch induced from shear forces, especially in the proximal direction [7-9].

The ability to sense normal and shear forces plays a critical role in the control of grip. Johansson et al. demonstrated that when grasping an object, the responses of SA-II units are strongly influenced by both skin indentation and lateral forces, thus they are presumed to contribute to the estimation of the load presented by a grasped object and the control of finger forces required to maintain grip [10, 11]. If the center of mass of a grasped object lies outside the points of contact with the object, the skin will experience a pattern of tangential torques that will be sensed by Ruffini endings [12].

B. Human physiology and grip control

When grasping an object, humans use slightly more force than required to prevent slip. The use of a safety factor is helpful to prevent slips from unexpected perturbations or to counteract torque that arises from off-centered loads. The presence of torque strongly influences the grip force required for grasp stability [13-15]. When controlling grip force, people take into account both tangential force and torque and as well as the shape of the object [15] and coefficient of friction in the object-digit interface. If the torque is excessive, humans naturally tend to set the object down and adjust their grip closer to the center-of-mass.

C. Artificial force and torque sensor and grip control

The majority of artificial tactile sensors sense normal force only but not shear force. Several groups have combined multiple normal-force sensors under both rigid and deformable contact elements to convert shear forces applied to the surface of the contact into normal forces at the base [16-20]. These work well only if the point of contact (PoC) is singular and well-known. They often require a relatively large number of sensing elements and their electrical connections, which may be difficult to provide on anything except a rigid, flat substrate such as used for MEMS arrays. Optical three-axis tactile sensors [16] are bulky and require image processing. Multiaxis force-plates can be used to extract 6DOF forces and torques as well as PoC if the surface is known [22], but they tend to be bulky and fragile.

II. The BioTac

A. Multimodal sensing modalities

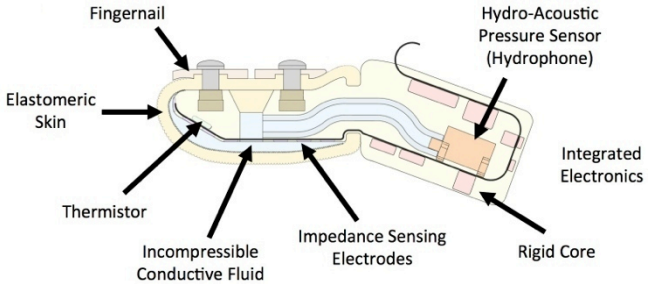

Figure 1 - Schematic diagram of the BioTac biomimetic tactile sensor. Contact with objects results in deformation of the elastomeric skin, which is sensed as impedance changes of the electrodes as the conductive fluid path changes. Other sensing modalities include static pressure and vibrations and temperature and thermal flux (thermistor).

C. H. Lin, is with SynTouch, LLC, Los Angeles, CA 90007 USA and the University Southern California, Los Angeles, CA 90007 USA (phone: 626-512-1579; e-mail: gary.c.lin@usc.edu).

J. A. Fishel is with SynTouch, LLC, Los Angeles, CA 90007 (e-mail: jeremy.fishel@syntouchllc.com).

G. E. Loeb, is with SynTouch, LLC, Los Angeles, CA 90007 USA and the Department of Biomedical Engineering at the University of Southern California, Los Angeles, USA 90089 USA (e-mail: gloeb@usc.edu).

Conflict of Interest Statement: Chia-Hsien Lin, Jeremy Fishel and Gerald Loeb are equity partners in SynTouch, LLC, which manufactures and sells the BioTac sensors described in this article.

The biomimetic mechanical properties and multimodal sensing of the BioTac are combined in a robust package that has been integrated onto various mechatronic grippers and hands. Figure 1 illustrates the basic design that supports the following three basic sensing modalities:

- **Contact points**, magnitude and direction of applied **forces** and **torques** distort the skin and liquid, resulting in distinctive and quantitative patterns of electrical impedance changes measured through the conductive liquid by nineteen active electrodes on the surface of the core (100 samples/s for each channel) [17, 18]. **Shear force** can be extracted from the bulging and compressing of the skin and fluid over lateral-facing electrodes [19].
- **Pressure** and **microvibrations** indicative of slip and texture of objects are detected by a MEMS pressure sensor in the liquid path (DC-20Hz @ 100 samples/s and 20Hz-1kHz @ 2000 samples/s) [20-23]
- **Temperature** and **heat flux** indicative of thermal properties of the contacted object are detected by a thermistor near the surface of the internally heated core (100 samples/s each) [24]

B. Previous studies using the BioTac for sensing force

Previous studies with the BioTac have relied on neural networks and machine learning to extract force, point of contact, and radius of curvature from electrode data. [18, 25]. While these methods yielded good results under their training conditions, they were not found to be robust enough for use in a wider range of conditions. In this study we developed and validated purely analytical approaches based on the geometry of the core and electrodes.

III. THEORY

A. Geometry of Electrodes

The BioTac contains 19 sensing electrodes (E1-E19) and four excitation electrodes (X1-X4) (Figure 2). When sampling an electrode, a voltage pulse is injected into the reference electrodes. The distributed excitation electrodes allow for multiple conductive pathways to each sensing electrode as it is sampled; this ensures that changes in sensed impedance of a given sensing electrode are due largely to deformation around the sensing electrode alone. The impedance between the excitation and sensing electrode forms the top of a voltage divider with a 10kΩ resistor whose voltage is digitized (12 bit resolution) in the BioTac. The resting impedance of each electrode tends to be 3-5 kΩ, rising to 10MΩ for maximal normal force of 30N. The signal is thus nonlinearly related to conductance in the liquid layer, which goes down when compressed but up from the resting value if the fluid layer bulges as a result of displacement from other parts of the BioTac. Because of the convex shape of the BioTac and the anchoring of the skin by the dorsal fingernail, shear forces produce such displacements away from the point of contact (PoC), as shown in Figure 3. Based on this observation, we develop simplified calculations of force and torque by assuming that each electrode measures force in the direction of its normal. This offers many advantages in simplified calculations that can be computed rapidly and eliminates the need for training data that would otherwise be required in previous machine learning methods [18, 25]. Data presenting the location and orientation of the 19 sensing electrodes and four excitation electrodes in Cartesian coordinates are provided in (Table 1).

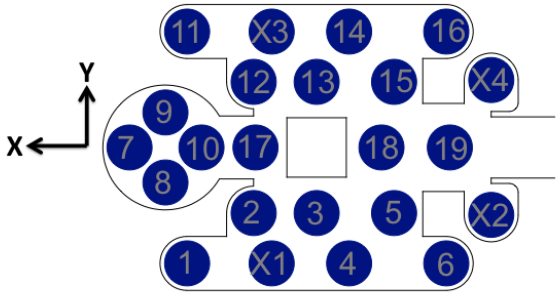

Figure 2 - Electrode array of the flex circuit shown as a flattened view of the compound convex surface.

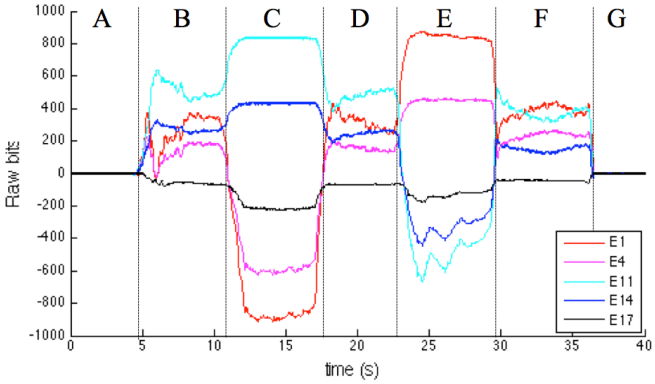

Figure 3 – Shear-force trial. A. electrode data normalized at rest; B. 500g weight (~5N) with a flat surface in the x-y plane balanced on BioTac surface; C. manually applied shear force (~3N) in positive y-direction added to weight; D. shear force removed; E. similar shear in negative y-direction; F. shear force removed; G. weight removed and electrodes automatically renormalized. Note that lateral electrode conductances (E1, 4, 11, 14) rise during initial contact as liquid is displaced towards them, while conductance of E17 under the weight is reduced throughout. Lateral facing electrodes E1 and E4 show changes whose sign depends on direction of tangential force; E11 and E14 on the opposite have reciprocal changes. Manually applied forces resulted in changes in normal force, as detected by E17.

	Coordinates ($\overrightarrow{R_e}$)			Normal Vector ($\overrightarrow{N_e}$)		
	x (mm)	y (mm)	z (mm)	X (n_x)	Y (n_y)	Z (n_z)
E1	0.993	-4.855	-1.116	0.196	-0.956	-0.220
E2	-2.700	-3.513	-3.670	0.000	-0.692	-0.722
E3	-6.200	-3.513	-3.670	0.000	-0.692	-0.722
E4	-8.000	-4.956	-1.116	0.000	-0.976	-0.220
E5	-10.500	-3.513	-3.670	0.000	-0.692	-0.722
E6	-13.400	-4.956	-1.116	0.000	-0.976	-0.220
E7	4.763	0.000	-2.330	0.500	0.000	-0.866
E8	3.031	-1.950	-3.330	0.500	0.000	-0.866
E9	3.031	1.950	-3.330	0.500	0.000	-0.866
E10	1.299	0.000	-4.330	0.500	0.000	-0.866
E11	0.993	4.855	-1.116	0.196	0.956	-0.220
E12	-2.700	3.513	-3.670	0.000	0.692	-0.722
E13	-6.200	3.513	-3.670	0.000	0.692	-0.722
E14	-8.000	4.956	-1.116	0.000	0.976	-0.220
E15	-10.500	3.513	-3.670	0.000	0.692	-0.722
E16	-13.400	4.956	-1.116	0.000	0.976	-0.220
E17	-2.800	0.000	-5.080	0.000	0.000	-1.000
E18	-9.800	0.000	-5.080	0.000	0.000	-1.000
E19	-13.600	0.000	-5.080	0.000	0.000	-1.000
X1	-3.700	-4.956	-1.116	0.000	-0.976	-0.220
X2	-15.900	-3.589	-3.595	0.000	-0.706	-0.708
X3	-3.700	4.956	-1.116	0.000	0.976	-0.220
X4	-15.900	3.589	-3.595	0.000	0.706	-0.708

Table 1 – Electrode orientation and location in 3D coordinates.

B. Point of Contact

The PoC is computed by a weighted average of the signals from all electrodes according to their Cartesian coordinates (from Table 1):

$$\langle x_c, y_c, z_c \rangle = \frac{\sum_{i=1}^{19} (|e_i^*|^n \langle x_i, y_i, z_i \rangle)}{\sum_{i=1}^{19} |e_i^*|^n} \quad [1]$$

Values from the electrodes are first normalized (e_i*) such that the output is equal to zero at rest. The absolute value of the changes is used to cancel the effects of any tangential forces on lateral electrodes, which are both negative and positive as a result of squeezing and bulging, respectively. These absolute-value changes are then raised to a power n so that the impedance values of the electrodes experiencing direct normal forces tend to dominate. The value of n controls the smoothness of transitions when the actual PoC is between electrodes. A high value of n would result in contact being determined at the single electrode with the highest value; this results in the PoC jumping from one electrode to another as contact shifts over the BioTac. A low value of n would result in undesirable contributions from adjacent electrodes where contact is not being made but the shape of the object may result in small, asymmetrical changes. In this study we found n=2 to be an optimal setting by direct experimentation.

The center computed by Eq. 1 often lies within the convex BioTac rather than on its surface; to correct for this it is shifted to the nearest point on the surface. We estimated the simplified geometry of the BioTac as a half-cylinder with a quarter-cylinder cap, both of the same radius r. Given the origin of the BioTac (which was selected as the center of the sphere) this adjustment could be made with the following equations for x>0 for the spherical region and x<0 for the cylindrical region.

$$\begin{aligned} &if\ x > 0 \ \rightarrow \langle x_c, y_c, z_c \rangle' = \langle x_c, y_c, z_c \rangle \frac{r}{\sqrt{x_c^2 + y_c^2 + z_c^2}} \\ &if\ x < 0 \ \rightarrow \langle x_c, y_c, z_c \rangle' = \langle x_c, \frac{y_c}{\sqrt{y_c^2 + z_c^2}}, \frac{z_c}{\sqrt{y_c^2 + z_c^2}} \rangle \end{aligned} \quad [2]$$

C. Force

As specified above, it was observed that each electrode was most responsive to compression along the electrode's normal. We calculate tri-axial force using this assumption by summing the normal vectors of each electrode weighted by e_i* (Eq. 3). A scaling value S_x that is independent for each dimension of force is used to convert the results to Newtons and was obtained through direct experimentation:

$$\vec{F} = \langle S_x \sum_{i=1}^{19} e_i n_{x,i}, S_y \sum_{i=1}^{19} e_i n_{y.i}, S_z \sum_{i=1}^{19} e_i n_{z,i} \rangle \quad [3]$$

D. Torque

Torque is computed from the cross product of force and the moment. Continuing with the assumption that each electrode is responsive to force normal to its electrode orientation, we calculate torque as the summation of torque from each electrode:

$$\vec{M} = \sum_{i=1}^{19} (\vec{r_i}) \times (e_i \vec{n_i}) \quad [4]$$

Here $\vec{r_i}$ and $\vec{n_i}$ are the location and orientation of each electrode. Each dimension of the torque is scaled to convert values to Newton-millimeters.

IV. Methods

A. Experiment setup

A BioTac mounted on a mechanical adapter that mated with to a 6 degree of freedom force plate (ATI Industrial Automation, Nano17) (Figure 4). Once installed, the skin was inflated to the proper specification of approximately 2mm liquid thickness. The flexible circuit of the BioTac was connected to the electrical adapter board and data were collected with the Cheetah SPI adapter (Total Phase Inc.). The 6 differential analog signal pairs from the Nano17 were digitized by USB-6218 DAQ system (National Instruments). A customized LabVIEW program controlled the sampling rate (electrodes: 100 samples/s each; Nano17: 1000 samples/s) and recorded the data, which were analyzed off-line (MathWorks, MATLAB).

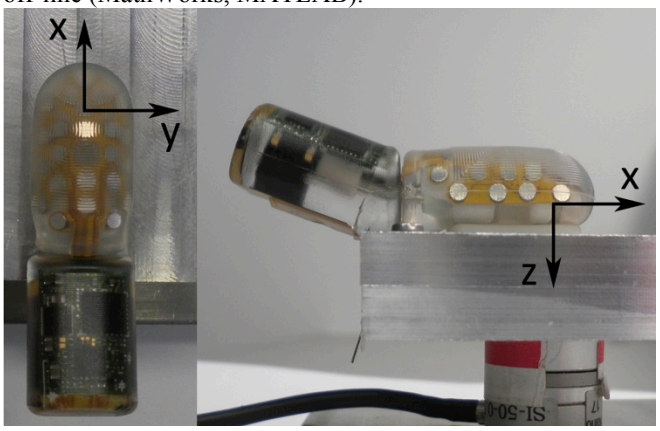

Figure 4 – Top and lateral views of the BioTac on force plate apparatus showing coordinate system.

B. Data collection

In all of the validation tests, the forces were applied by hand and the estimates from the BioTac were compared to the computations from the force-plate data. For the PoC estimates, forces were applied via a 2mm diameter, flat-tipped probe directly over each electrode (as seen through the transparent skin). For the tangential force and torque estimates, stimuli were applied via a weight of 500g with a large flat surface in a single orientation in the x-y plane; rotational torques were applied manually in the plane of contact.

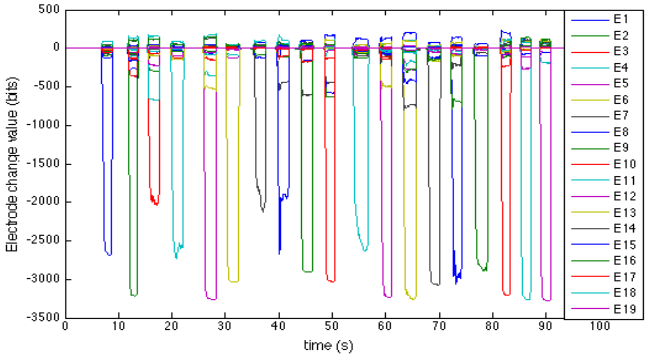

Figure 5 – BioTac normalized electrodes values in electrodes poking task. The electrode poking sequence is same as electrode numbering.

To deal with drifting electrode values, all electrode signals were renormalized between each contact. A 100ms window was used to tare the measured values if the change in impedance was small or drifting. The threshold was set to 1000bit^2, equivalent to roughly 0.5N. This accounted well for drift yet still permitted slow loading of the BioTac without incorrectly zeroing the signals (see Fig. 5 for example of renormalization between pokes in the PoC test).

C. Computations from force plate data

To calculate a frame of reference for point of contact, force, and torque computed from impedance data, we used methods from [26] to estimate these same parameters from force plate data. Without friction, the force at the point of contact must be normal to the surface, but with friction, shear forces and torques can arise. However, without adhesion the torque at the contact point must be purely normal to the surface. Therefore, to estimate the contact location C we determine the point where the moment parallel to the surface is minimized by the following equation:

$$C \ni \min\left(\vec{n}\times\overrightarrow{M_c}\right) \quad [5]$$

When maintaining the same coordinate frame, the moment from the origin of the force plate can be transposed to a new origin using the following equation:

$$\overrightarrow{M_c} = \overrightarrow{M_o} + \vec{r}\times\vec{F} \quad [6]$$

A mesh with approximate spacing of 0.5mm was created for the BioTac to find this local minimum. We assume that the geometry of the BioTac consists of a half-cylinder with a quarter-sphere at the tip (Figure 6) in order to compute a point that satisfies this equation.

$$z = \begin{cases} -\sqrt{a^2 - y^2}, & x < 0 \text{ (cylinder region)} \\ -\sqrt{a^2 - x^2 - y^2}, & x \geq 0 \text{ (sphere region)} \end{cases} \quad [7]$$

Where $a = 5.08mm$.

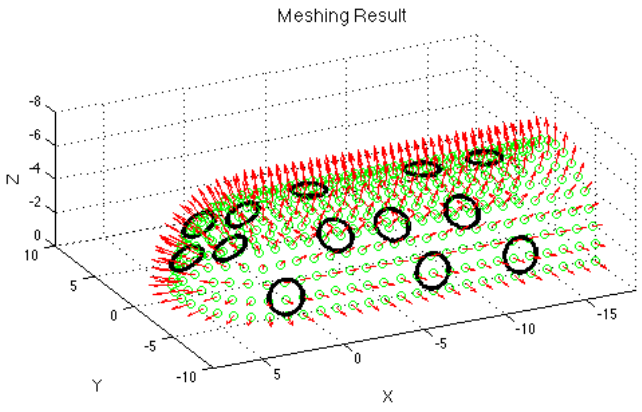

Figure 6 – The BioTac mesh and electrode locations. Green circles are meshing points with approximate spacing of 1mm. Red arrows are the normal vectors to the surface. Big black circles are electrode positions (only E1-E10, and E17-E19 shown in the figure)

V. Results

A. Point of contact (PoC) validation

Results of determining point of contact from the electrode poking test are shown in Figure 7. PoC estimates from the BioTac (blue circles) are clustered around actual electrode locations, while the contact points estimated from the force plate (green circles) are less precise. Table 2 shows the two different trials with their standard deviations from these two methods. In general, using electrode data from the BioTac to determine contact location was found to be more accurate and significantly more precise than using the force plate. This is presumably because the sensing electrodes on the surface of rigid core are influenced directly to the skin deformation while the computational model has errors related to signal-to-noise values and uncertainties in the computational model. PoC estimates from the BioTac were relatively reliable when the applied force exceeded 1N.

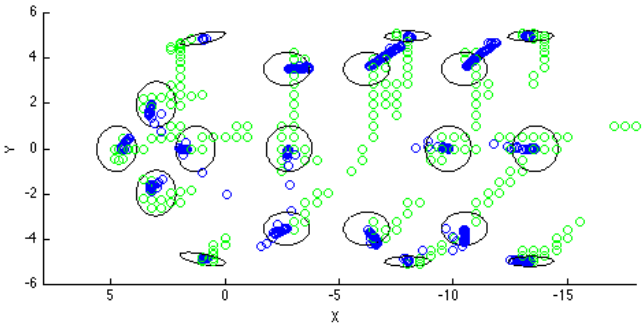

Figure 7 – Point of contact result from electrodes poking task of all 19 electrodes (locations at the black circles). Methods using the impedance data from the BioTac (blue circles) are shown to be more precise and accurate than methods using the force plate data (green circles).

	BioTac Trail 1	BioTac Trail 2	Nano17 Trail 1	Nano17 Trail 2
E1	0.0388	0.0065	0.6016	0.6112
E2	0.2452	0.1911	0.3788	0.5310
E3	0.1118	0.0959	0.4881	0.3337
E4	0.0208	0.0157	0.5026	0.2973
E5	0.3911	0.2059	3.0020	0.2133
E6	0.0695	0.0585	0.5849	0.2078
E7	0.0690	0.4027	0.6663	0.7474
E8	0.0681	0.4383	0.3622	0.6417
E9	0.1527	0.7310	0.3694	0.6289
E10	0.5356	1.5708	0.4546	0.3619
E11	0.0076	0.0095	0.8817	0.1037
E12	0.1088	0.5052	1.0673	0.6312
E13	0.6269	0.1208	1.2259	0.5566
E14	0.0122	0.1038	1.6051	1.4153
E15	0.8159	0.1136	1.1535	0.2669
E16	0.0057	0.0404	1.0251	0.2760
E17	0.6191	1.5448	0.1842	0.0965
E18	0.1643	0.2959	0.1555	3.1193
E19	0.2477	0.3525	0.1491	0.4673
Average	**0.2269**	**0.3580**	**0.7820**	**0.6056**

Table 2 – Point of Contact standard deviation comparison. Unit: mm

B. Force and torque calculation

1) Electrode poking task

When applying force to a single electrode with a small probe the resulting force and moment estimations were found to be accurate when scaled properly (Figure 8).

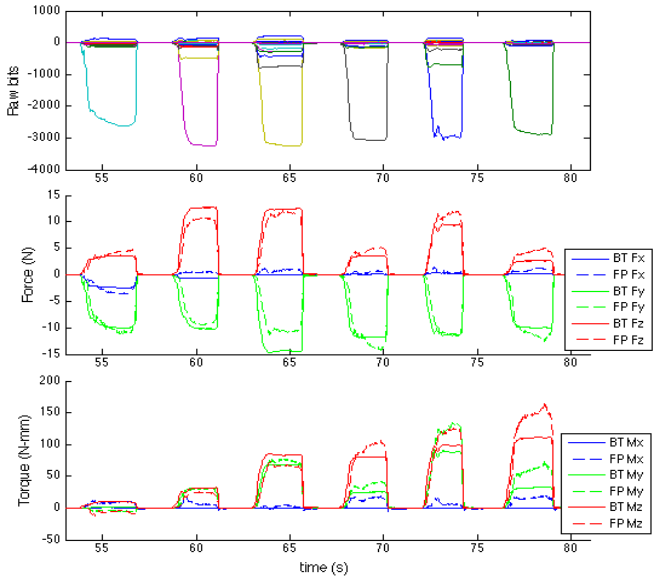

Figure 8 – E11-E16 Electrode poking data A) BioTac normalized electrodes values in electrode poking task. The electrodes poking sequence is same as electrodes numbering. B) Force calculation from BioTac (solid line) and Nano17 force plate (dash line). C) Torque calculation

2) Tangential torque validation

Each trial was divided into seven phases (A-G, Figure 9):

A. Resting phase –no loads; electrode readings normalized.

B. Loading phase –flat 500g weight (~5N in z-axis) applied to the x-y plane of the BioTac and held for ~5s.

C. A clockwise torque is applied for ~5s

D. The torque is removed; weight at rest for ~5s.

E. A counter-clockwise torque is applied for ~5s.

F. The torque is removed; weight at rest for ~5s.

G. Unloading phase –weight removed; electrodes renormalized.

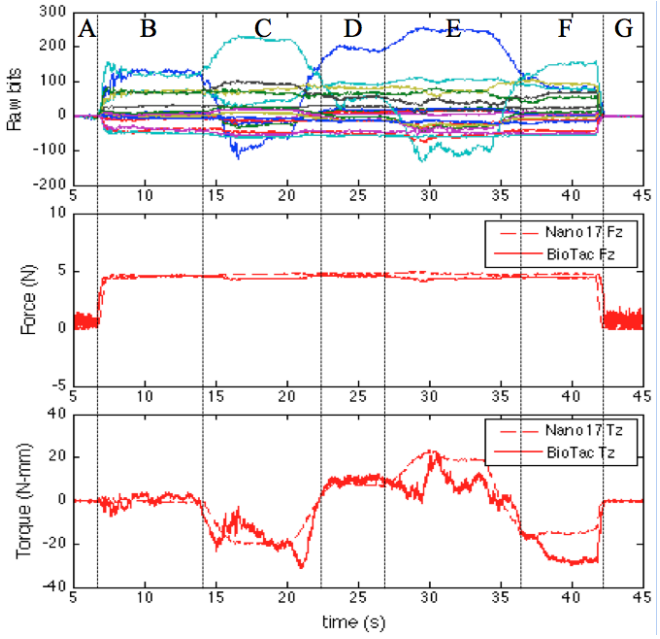

Figure 9 - Top: 19 normalized electrode readings; see text for lettered phases. Middle: comparison of z-axis force estimated from BioTac and computed from force plate. Bottom: comparison of z-axis torque estimated from BioTac and computed from force plate.

3) Rotation task with additional shear force

When tangential force and torques were presented simultaneously, the estimates of each from the BioTac data were substantially convolved. Region II in Figure 10 represents a sequence similar to the tangential torque test in Figure 9; region I shows the same torque sequence during manually added shear force in positive y-direction; region III is during shear in negative y-direction.

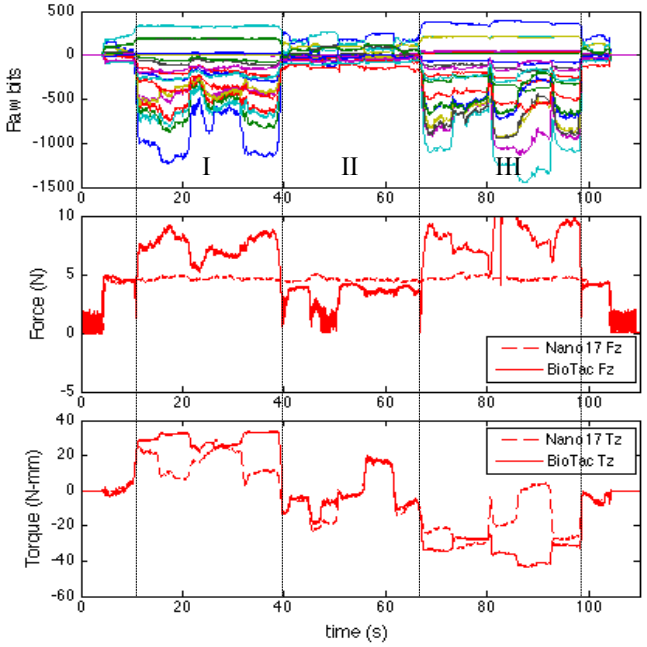

Figure 10 – Traces similar to Figure 9; see text for description of regions I, II, III.

VI. Discussion

In this study we presented analytical estimates of forces, torques and point of contact from BioTac electrode measurements and characterized their performance compared to a commercial 6DOF force-plate. The analytical method is not subject to over-training and instability problems common to neural networks. The analytical method successfully extracted pure tangential torques, which has not been done before. The interactions between tangential forces and torques are not yet understood but may be correctible with an improved analytical model. In particular, there are two sources of asymmetry that are not included in the model: I) The finger-shaped BioTac is not radially symmetrical, as assumed by the analytical solution. II) Compression of the liquid space tends to produce larger changes in electrode readings than comparably sized bulges in the liquid space.

To compensate for the hysteresis of the electrodes, we successfully implemented a function to compensate the electrode value-drifting problem. This function can be used on-line to overcome effects apparently related to skin hysteresis. Previous studies of hysteresis in the BioTac were limited to purely normal force loading and showed negligible values (~3% over the full dynamic range) [24]. Loading the skin with large tangential forces and torques probably produces small shifts in the fixation of the skin at the fingernail and o-ring seals, which can be corrected by the normalization algorithm employed in this study.

REFERENCES

[1] A. B. Vallbo and R. S. Johansson, "Properties of cutaneous mechanoreceptors in the human hand related to touch sensation," *Hum. Neurobiol.,* vol. 3, pp. 3-14, 1984.

[2] R. S. Johansson and J. R. Flanagan, "Somatosensation," in *The Senses: a Comprehensive Reference*. vol. 6, E. Gardner and J. H. Kaas, Eds., ed San Diego: Academic Press, 2008, pp. 67-86.

[3] L. A. Jones and S. J. Lederman, "Human Hand Function," ed. Oxford, England, 2006.

[4] M. A. Srinivasan, J. M. Whitehouse, and R. H. LaMotte, "Tactile Detection of Slip: Surface Microgeometry and Peripheral Neural Codes," *Journal of Neurophysiology,* vol. 63, pp. 1323-1332, 1990.

[5] G. Westling and R. S. Johansson, "Factors Influencing the Force Control During Precision Grip," *Experimental Brain Research,* vol. 53, pp. 277-284, 1984.

[6] J. R. Phillips and K. O. Johnson, " Tactile spatial resolution: II. Neural representation of bars, edges, and gratings in monkey primary afferents," *Journal of Neurophysiology,* vol. 46, pp. 1192–200, 1981.

[7] I. Birznieks, P. Jenmalm, A. W. Goodwin, and R. S. Johansson, "Encoding of direction of fingertip forces by human tactile afferents," *J.Neurosci.,* vol. 21, pp. 8222-8237, 2001.

[8] K. O. Johnson, Y. T., and F. Vega-Bermudez, "Tactile functions of mechanoreceptive afferents innervating the hand," *Journal of Clinical Neurophysiology,* vol. 17, pp. 539-558, 2000.

[9] H. Olausson, J. Wessberg, and N. Kakuda, "Tactile directional sensibility: peripheral neural mechanisms in man," *Brain Res.,* vol. 866, pp. 178-87, 2000.

[10] R. S. Johansson and G. Westling, "Signals in tactile afferents from the fingers eliciting adaptive motor responses during precision grip," *Experimental Brain Research,* vol. 66, pp. 141-154, 1987.

[11] G. Westling and R. S. Johansson, "Responses in glabrous skin mechanoreceptors during precision grip in humans," *Experimental Brain Research,* vol. 66 pp. 128-140, 1987.

[12] A. M. Wing and S. L. Lederman, "Anticipating load torques produced by voluntary movements. ," *Journal of Experimental Psychology: Human Perception and Performance,* vol. 24, pp. 1571-1581, 1998.

[13] H. Kinoshita, L. Bäckström, J. R. Flanagan, and R. S. Johansson, "Tangential torque effects on the control of grip forces when holding objects with a precision grip," *Journal of Neurophysiology,* vol. 78, pp. 1619-1630, Sep 1997.

[14] A. W. Goodwin, P. Jenmalm, and R. S. Johansson, "Control of grip force when tilting objects: Effect of curvature of grasped surfaces and applied tangential torque," *Journal of Neuroscience,* vol. 18, pp. 10724-10734, 1998.

[15] B. B. Edin, G. Westling, and R. S. Johannson, "Independent control of human finger-tip forces at individual digits during precision lifting," *Journal of Physiology,* vol. 450, pp. 547-564, 1992.

[16] M. Ohka, Y. Mitsuya, and S. Takeuchi, "Sensing characteristics of an optical three-axis tactile sensor under combined loading," *Robotica,* vol. 22, pp. 213-221, 2004.

[17] N. Wettels, V. J. Santos, R. S. Johansson, and G. E. Loeb, "Biomimetic Tactile Sensor Array," *Advanced Robotics,* vol. 22, pp. 829-849, 2008.

[18] N. Wettels and G. E. Loeb, "Haptic feature extraction from a biomimetic tactile sensor: Force, contact location and curvature," in *Robotics and Biomimetics (ROBIO), 2011 IEEE International Conference on*, 2011, pp. 2471-2478.

[19] Z. Su, J. A. Fishel, T. Yamamoto, and G. E. Loeb, "Use of tactile feedback to control exploratory movements to characterize object compliance," *Frontiers in Neurorobotics,* vol. 6, 2012.

[20] J. A. Fishel, V. J. Santos, and G. E. Loeb, "A robust micro-vibration sensor for biomimetic fingertips," in *Biomedical Robotics and Biomechatronics, 2008. BioRob 2008. 2nd IEEE RAS & EMBS International Conference on*, 2008, pp. 659-663.

[21] N. Wettels, J. A. Fishel, Z. Su, C. H. Lin, and G. E. Loeb, "Multi-modal Synergistic Tactile Sensing," in *Tactile Sensing in Humanoids- Tactile Sensors and Beyond Workshop, 9th IEEE-RAS International Conference on Humanoid Robots.*, 2009.

[22] J. A. Fishel and G. E. Loeb, "Bayesian exploration for intelligent identification of textures," *Frontiers in Neurorobotics,* vol. 6, 2012.

[23] J. A. Fishel and G. E. Loeb, "Sensing Tactile Microvibrations with the BioTac – Comparison with Human Sensitivity," presented at the IEEE/RAS-EMBS International Conference on Biomedical Robotics and Biomechatronics, Rome, 2012.

[24] C. H. Lin, T. W. Erickson, J. A. Fishel, N. Wettels, and G. E. Loeb, "Signal Processing and Fabrication of a Biomimetic Tactile Sensor Array with Thermal, Force and Microvibration Modalities," in *IEEE International Conference on Robotics and Biomimetics*, 2009.

[25] N. Wettels, A. R. Parnandi, J. Moon, G. E. Loeb, and G. S. Sukhatme, "Grip control using biomimetic tactile sensing systems," *IEEE/ASME Transactions on Mechatronics,* vol. 14, pp. 718-723, 2009.

[26] A. Bicchi, J. K. Salisbury, and D. L. Brock, "Contact Sensing from Force Measurements," *International Journal of Robotics Research,* vol. 12, pp. 249-262, 1993.